A&A 475, 539–547 (2007)
DOI: 10.1051/0004-6361:20078341

Astronomy & Astrophysics

Lithium abundances in the old open cluster NGC 3960 from VLT/FLAMES observations⋆,⋆⋆

L. Prisinzano[1] and S. Randich[2]

[1] INAF – Osservatorio Astronomico di Palermo, Piazza del Parlamento 1, 90134 Palermo, Italy
e-mail: loredana@astropa.inaf.it
[2] INAF – Osservatorio Astronomico di Arcetri, Largo E. Fermi 5, 50125 Firenze, Italy
e-mail: randich@arcetri.astro.it

Received 24 July 2007 / Accepted 7 September 2007

ABSTRACT

Context. Old open clusters are very useful targets to investigate mechanisms responsible for lithium (Li) depletion during the main sequence. Comparison of the Li abundances in clusters of different age allows us to understand the efficiency of the Li destruction process.
Aims. To determine the membership and Li abundance in a sample of candidate members of the open cluster NGC 3960 (age ∼1 Gyr), aiming to fill the gap between 0.6 and 2 Gyr in the empirical description of the behavior of the average Li abundance as a function of the stellar age.
Methods. We use VLT/FLAMES Giraffe spectra to determine the radial velocities and thus the membership of a sample of 113 photometrically selected candidate cluster members. From the analysis of the Li line we derive Li abundances for both cluster members and non-members.
Results. 39 stars have radial velocities consistent with membership, with an expected fraction of contaminating field stars of about 20%. Li is detected in 29 of the radial velocity members; we consider these stars as cluster members, while we make the reasonable assumption that the remaining 10 radial velocity members without Li are among the contaminating stars. Li abundances of the stars hotter than about 6000 K are similar to those of stars in the Hyades, while they are slightly smaller for cooler stars. This confirms that NGC 3960 is older than the Hyades.
Conclusions. The average Li abundance of stars cooler than about 6000 K indicates that the Li Pop. I plateau might start at ∼1 Gyr, rather than 2 Gyr, which is the upper limit previously derived in the literature. We also find that the fraction of field stars with high Li abundance ($\gtrsim$1.5) is about one third of the whole sample, which is in agreement with previous estimates. The fraction of contaminating field stars is consistent with that previously derived by us from photometry.

Key words. stars: abundances – stars: evolution – Galaxy: open clusters and associations: individual: NGC 3960

1. Introduction

Open cluster (OCs) are commonly recognized as one of the best tools to investigate the formation and evolution of the Galactic disk, as well as the evolution of stars and their properties.

We have carried out a VLT/FLAMES project aimed at deriving homogeneous information for a sample of 11 old OCs (ages greater than about 0.9 Gyr) with the aim of a) deriving their chemical composition from UVES spectra of evolved stars, and b) determining their radial velocities and thus membership, together with lithium (Li) abundances from Giraffe spectra of turn-off (TO) and main sequence (MS) cluster candidates (Randich et al. 2005; Pallavicini et al. 2006). In this paper we focus on Giraffe observations of NGC 3960, the youngest OC in our sample.

In the last few years, this cluster has been the object of different photometric and spectroscopic studies, which have allowed a more accurate determination of its parameters. Bragaglia et al. (2006) derived an age between 0.6 and 0.9 Gyr, a distance modulus $(m-M)_0 = 11.6 \pm 0.1$, a reddening $E(B-V) = 0.29 \pm 0.02$, with differential reddening $\Delta E(B-V) = 0.05$. A slightly older age (in the range 0.9–1.4 Gyr) was derived by Prisinzano et al. (2004) who also estimated the cluster mass function from the luminosity function in the V and J bands, finding a slope $\alpha = 2.95 \pm 0.53$ for masses above 1 $M_\odot$. Note that the contamination from field stars was taken into account using a control field and performing a statistical subtraction. A spectroscopic [Fe/H] = −0.12 ± 0.04 was derived by Bragaglia et al. (2006), while Sestito et al. (2006) report a slightly higher value [Fe/H] = 0.02 ± 0.04: in both cases the metallicity is consistent with the solar value.

Given its age (we assume here 0.9 Gyr), NGC 3960 provides a good sample to investigate the evolution of lithium abundance during the MS and, in particular, to fill the gap in age coverage between the Hyades (0.6 Gyr) and the ∼1.5–2.0 Gyr clusters for which Li data are available (NGC 752, IC 4651).

Sestito & Randich (2005) investigated the timescales for Li depletion during the MS for F and G–type stars, by means of a homogeneous re-analysis of Li data for several open clusters. They suggested that Li depletion is not a continuous process, but is instead characterized by different timescales in different age intervals. In particular, they showed that Li depletion slows down after the Hyades age for stars in the temperature range ∼6050–6350 K, while it stops for cooler stars. Namely, for stars

⋆ Based on observations collected at ESO-VLT, Paranal Observatory, Chile, Programme numbers 73.D-0520(A)
⋆⋆ Table 4 is only available in electronic form at http://www.aanda.org

cooler than ∼6050 K, a plateau in Li abundance is seen for ages older than ∼2 Gyr; this age, however, represents an upper limit to the actual age when Li depletion is no longer efficient. A more precise estimate of this age, which would provide a useful constraint to models including extra-mixing during the MS, requires Li data for clusters with ages between 0.6–2 Gyr. We also mention in passing that since the study of Sestito & Randich (2005) has been used to infer the age of stars hosting extra-solar planets (e.g. Sozzetti et al. 2007), a finer sampling of the 0.6–2 Gyr interval would allow these stars to be age dated with higher accuracy.

Besides allowing measurements of Li abundances, our Giraffe spectra have been used to determine radial velocities and cluster membership for the observed candidates. This in turn will allow us to perform a revised analysis of contamination from field stars and cluster mass function.

Our paper is structured as follows: in Sect. 2 we describe the criterion adopted to select the spectroscopic targets and observations, and in Sect. 3 we report the analysis of the spectra, including the procedure used to derive the radial velocity (*RV*) and the equivalent width (*EW*) of the Li line. In Sect. 4 we describe how we derive the effective temperatures and the Li abundances of our targets. In Sect. 5, we discuss the Li abundances for both the cluster members and the field stars, by comparing our results with those of stars of similar spectral type taken from literature. We also compare the fraction of contaminating field stars in the spectroscopic sample with that previously obtained statistically from photometric data. Our conclusions are presented in Sect. 7.

2. Target selection and observations

The targets observed with VLT/FLAMES were retrieved from the photometric catalog of Prisinzano et al. (2004), selecting objects in the cluster region, i.e., within 7′ from the cluster centroid. In total, we observed 113 candidate members on the MS with $16 \leq V \leq 18$, corresponding to spectral–types from F to early K: stars with V larger than 18 are too cool and faint to reach a S/N ratio larger than 40, which is required to accurately measure the *RV*s and *EW*s; stars brighter than 16 are hotter than early F stars and therefore are not good targets to investigate Li depletion in old MS stars.

In Fig. 1 we show the V vs. $V-I$ color-magnitude diagram for the region within 7′ from the centroid of NGC 3960 (dots) where photometry is corrected for differential reddening.

The observations were carried out in Service Mode during February, March and April 2004; the log of the observations is provided in Table 1. The cluster was covered by one configuration centered at RA(2000) = $11^{\rm h}50^{\rm m}31^{\rm s}.400$ Dec(2000) = $-55°41'12''.80$. Giraffe was used in conjunction with the 316 lines/mm grating and order sorting filters 14 (HR14) and 15 (HR15), yielding nominal resolving powers R = 28 800 and 19 300, respectively. Spectral coverages are from 630.8 to 670.1 for HR14 and from 660.7 to 696.5 nm for HR15; they include Hα, the Li I 670.8 nm line and several features to be used for *RV* measurements. For each set-up, four 45 min exposures were obtained.

Data reduction was carried out using the GIRAFFE BLDRS pipeline[1], following the standard procedure and steps (Blecha & Simond 2004). Sky subtraction for the spectrum of each set-up and each exposure was performed separately, namely by subtracting the median, computed as in Jeffries & Oliveira (2005), of the 16 sky fiber spectra observed in the same exposure. The four

[1] Version 1.0 – `http://girbldrs.sourceforge.net/`

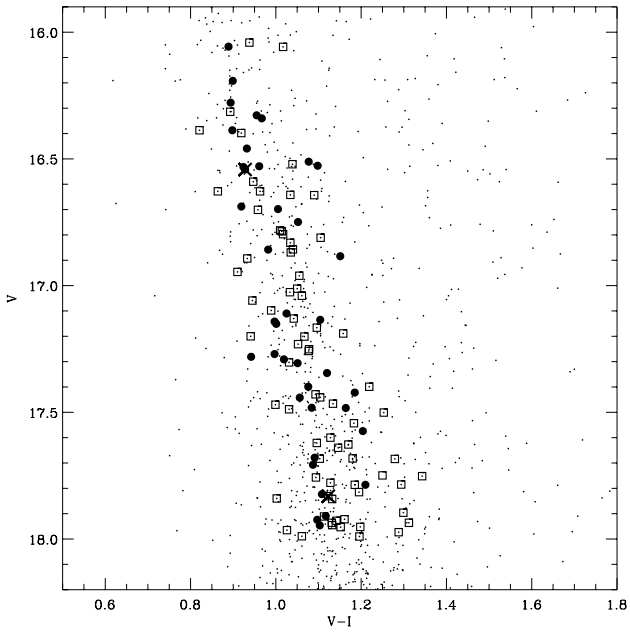

Fig. 1. Color-magnitude diagram for the region within 7′ from the centroid of NGC 3960 (dots). Photometry is from Prisinzano et al. (2004) and it is corrected for differential reddening. Targets observed with VLT/FLAMES are indicated with large symbols: filled circles are those with *RV* consistent with that of the cluster and empty squares are non-members having the *RV* different from the cluster members (see Sect. 3.1.1). The two stars indicated with the X symbols are candidate spectroscopic binaries (SB2).

Table 1. Log-book of Giraffe/FLAMES observations. Columns 1–4 give the observation date, original name associated with each observing block, exposure time, and grating used for each exposure, respectively.

Obs. Date	Exp. Name	Exp. Time (s)	Grating
04/03/2004	M1-Li-a	2700	HR15
04/03/2004	M2-Li-a	2700	HR15
04/03/2004	M2-Li-c	2700	HR15
04/20/2004	M1-ha	2700	HR14
05/02/2004	M1-Li-b	2700	HR15
05/02/2004	M2-ha-a	2700	HR14
05/02/2004	M2-ha-b	2700	HR14
05/20/2004	M2-ha-c	2700	HR14

sky-subtracted spectra of each target obtained with the HR15 set-up were then co-added, after applying the Doppler correction due to the different date of observations. Examples of final co-added sky-subtracted spectra around the Li line are shown in Fig. 2. S/N ratios are ∼80 for the stars OC21-M342 and OC21-M42 and ∼55 for OC21-M205 and OC21-M359. Final S/N ratios range between 30 and 80, as estimated from the faintest and the brightest stars in our sample.

3. Data analysis

3.1. Radial velocities

*RV*s in the heliocentric system of the 8 sets of spectra were computed using the function `giCrossC` of the GIRAFFE girBLDR pipeline. We computed the cross-correlation function between all the observed spectra and the synthetic template spectrum girKO corresponding to a K0V star. We used a delta *RV* limit to the cross-correlation window of 500 km s^{-1} in the wavelength

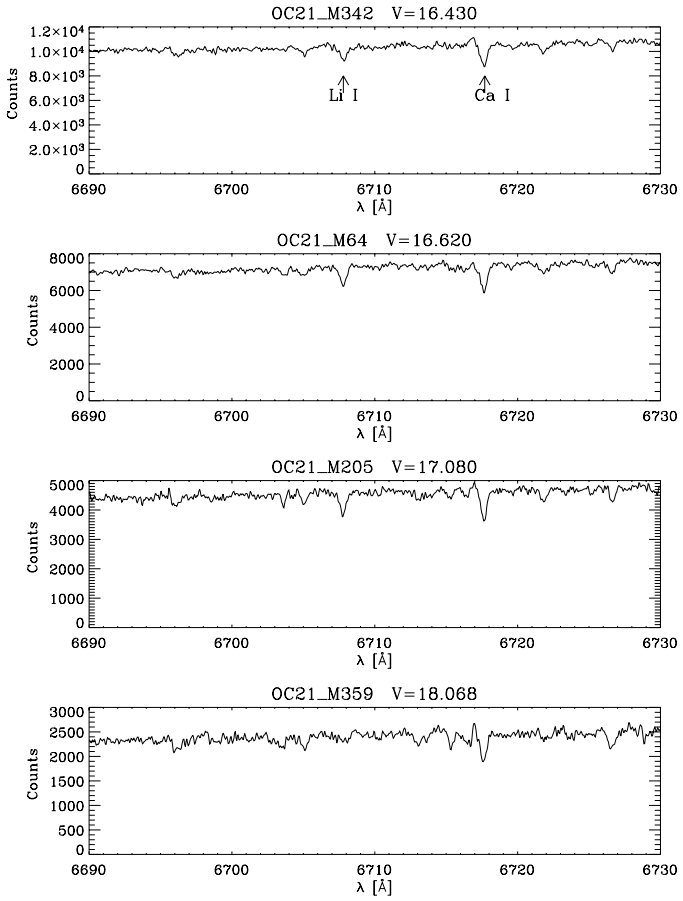

Fig. 2. Examples of co-added sky-subtracted spectra in the spectral region that includes the Li line. The GIRAFFE ID given in Table 4 and the *V* magnitude of the stars are indicated.

ranges [6310–6680] Å, for the spectra around the Li line, and [6610–6810] Å, for the spectra around the Hα line.

Final *RV*s for the stars of our sample were computed as the mean value and the standard deviation of the *RV*s obtained with `giCrossC` from the 8 different sets of spectra.

The *RV*s obtained using the function `giCrossC` as described before were compared with those obtained by using a different template spectrum, girG2, which corresponds to a spectrum of a solar-type star. The comparison does not evidence significant differences. In addition, in order to check the reliability of the automatic cross-correlation performed by the pipeline, we computed the *RV* for 4 of the 8 sets of spectra using the IRAF[2] task `FXCOR` (Tonry & Davis 1979); as template we used the spectrum of a relatively bright star ($V = 16.5$, spectral type F8V) from our sample, which is considered a reliable cluster member, based on its *RV* as measured with `giCrossC`. The relative *RV*s computed with `FXCOR` were converted into the heliocentric system using the heliocentric *RV* of the template star computed with `giCrossC`. The median of the differences between the four sets of *RV*s obtained with `giCrossC` *RV*s minus `FXCOR` *RV*s are 0.13, –0.34, 0.12 and –1.05 Km s^{-1}, while the standard deviations are 2.13, 2.16, 1.81 and 2.10 Km s^{-1}. Such values indicate an excellent agreement between the two methods. The difference between the mean *RV*s obtained with the two methods shows that only 8 stars (OC21-M80, OC21-M273, OC21-M581, OC21-M324, OC21-M282, OC21-M185, OC21-M177, OC21-M41) have a difference in the mean *RV* obtained with the two methods larger than 5 km s^{-1} and only 2 (OC21-M80 and OC21-M282) have a difference larger than 10 km s^{-1}. These objects do not show the Li line and 7 of them are not cluster members since they have a *RV* not consistent with that of the cluster (see next section). The only star classified as a cluster member (OC21-M273) based on its *RV* does not show the Li line and therefore it is considered a contaminating field star.

For 2 stars (OC21-M286, OC21-M136) the peak of the cross-correlation function performed with `FXCOR` is not symmetric but shows a double peak, which indicates that these objects are double-lined spectroscopic binaries (SB2). An inspection of the spectrum of these objects confirms the double spectral features, typical of SB2 stars.

3.1.1. Cluster membership

The density distribution of the final *RV*s is shown in the histogram of Fig. 3, where a significant peak around $RV = -20$ km s^{-1} indicates the presence of the cluster with respect to the *RV* distribution of the field stars, which shows a secondary peak at about -2 km s^{-1}.

To derive the cluster membership based on the *RV* we fitted the final *RV* distribution with a double Gaussian using the "maximum likelihood fitting", as in Prisinzano et al. (2007). We find that the cluster Gaussian is centered on -20.0 ± 0.7 km s^{-1} with a standard deviation $\sigma = 2.3 \pm 0.6$ km s^{-1}, while the much broader field star *RV* distribution shows a peak at -2.1 ± 2.6 km s^{-1}, with a standard deviation of $\sigma = 22.9 \pm 1.8$ km s^{-1}. The fitted curve is indicated by the solid line in Fig. 3. We note that the average cluster *RV* is smaller than the mean *RV* of NGC 3960 (equal to about -12 km s^{-1}) computed from 5 members studied in Friel & Janes (1993), but in very good agreement with the value derived by Sestito et al. (2006) from UVES spectra (-22.6 ± 0.9 km s^{-1}).

The total number of possible cluster members within $\pm 3\sigma$ of the cluster *RV* distribution is 39 including 16 contaminating field stars, as computed from the Gaussian distribution of the field stars. We note that some of the classified non-members could be spectroscopic binaries of the cluster, which cannot be easily distinguished from true non-members. From an inspection of the single spectra, only two objects, indicated by X symbols in Fig. 1, have been recognized from the characteristic double-line spectrum typical of SB2 stars (see Sect. 3.1).

Note that the identification of the cluster members does not allow us to reduce the spread in the CMD since the differential reddening corrections are computed using the reddening map shown in Fig. 8 of Prisinzano et al. (2004), which gives the *relative* reddening values in subregions of $1\farcm7 \times 1\farcm7$, with respect to the subregion where the cluster centroid is located. They are therefore spatially-dependent corrections and are not calculated for each star individually. This statistical method also includes the contaminating field stars. Individual spectral type estimates from low resolution spectra are needed to derive the individual reddening and thus the accurate position of the members in the CMD.

3.2. Li equivalent widths

Li *EW*s were measured on the co-added spectra normalized to their continuum. The normalization was performed using the region of the spectrum between 6693 and 6722 Å that includes the

[2] IRAF is distributed by the National Optical Astronomical Observatories, which are operated by the Association of Universities for Research in Astronomy, under contract with the National Science Foundation.

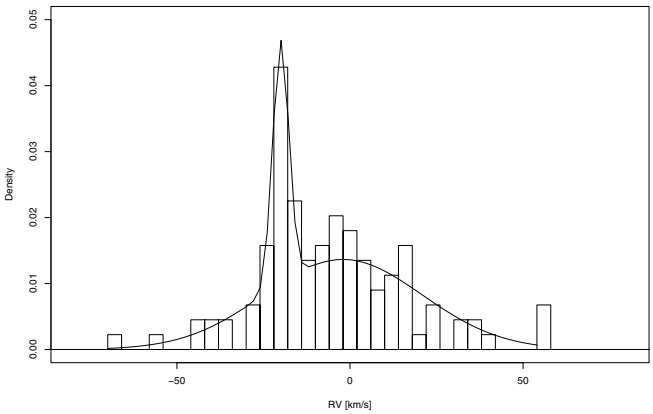

Fig. 3. Density distribution of the *RV* of the whole sample, which includes 113 stars. The fitted double Gaussian (see text) is indicated by the solid line.

Li I 6707.8 Å line; we used the IRAF task `CONTINUUM` with a second order Legendre function and a variable residual rejection limit chosen based on the visual inspection of the fitting result. The *EW*s of the Li I 6707.8 Å line were measured using the IRAF task `SPLOT`, assuming a Gaussian profile, which is a good approximation since the *EW*s are all smaller than about 100 mÅ and therefore the line is not saturated.

The continuum normalization and the *EW* measurements were repeated three times, on different dates; the continuum has been estimated by choosing each time a different residual rejection limit, that causes a change of the continuum level; different measures have been done after few months and therefore they are quite different. The mean of the three measurements was taken as the final estimation of the *EW*, and the maximum uncertainty was used as the error. We detected the Li line in 55 objects, 29 with *RV*s that were consistent with membership and 26 with *RV*s corresponding to non-members. Among the remaining 58 stars, we have 56 single objects and two SB2 binaries. For the 56 single stars, we estimated an upper limit of the *EW* by measuring the *EW* of the smallest line around 6707.8 Å. In some cases the spectra are of candidate M dwarf stars and show large molecular bands around the Li line. For these stars, we considered the whole depression of the spectrum, which includes the Li line, therefore the upper limits are very conservative.

We corrected measured *EW*s for the contribution of the Fe I line at 6707.44 Å using the relation $EW(\mathrm{Fe}) = 20(B-V)_0 - 3$ mÅ, given in Soderblom et al. (1993a) for stars with solar metallicity, thus appropriate for our cluster (Sestito et al. 2006).

Figure 4a shows the Li *EW*s measured for all of the 55 objects where Li was detected as a function of the dereddened $(B-V)$ colors, corrected for differential reddening, as described in Prisinzano et al. (2004). Figure 4b shows the Li *EW*s for the stars that are cluster members based on their *RV*, while Fig. 4c shows the Li *EW*s for the non-members. Upper limits are also plotted in the three panels, as well as Li *EW*s measured for the stars in the Hyades (Soderblom et al. 1990; Thorburn et al. 1993; Soderblom et al. 1995) .

Whereas our measurements are characterized by a larger spread, Fig. 4b indicates that the Li *EW*s of *RV* members are on average smaller than those of the Hyades members of similar color. This is also true for most of the *RV* non-members (Fig. 4c) with $(B-V)_0$ smaller than about 0.6 (F and G-type stars), while for redder colors, Li *EW*s are more comparable with those of Hyades stars.

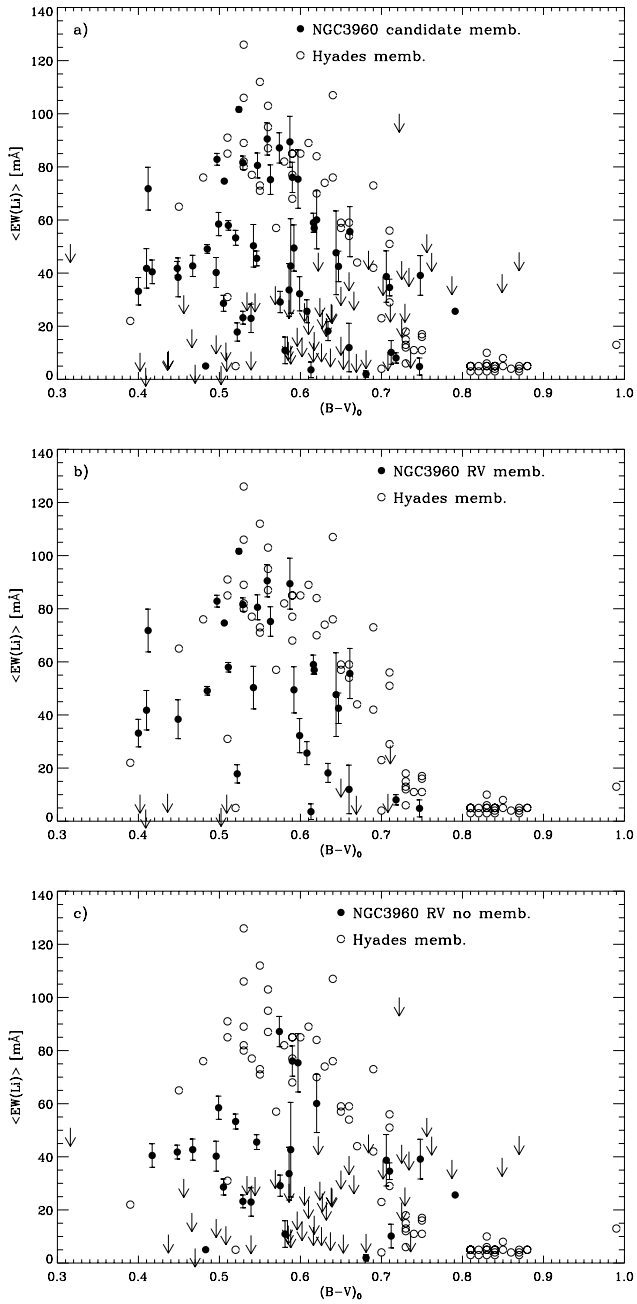

Fig. 4. a) Li *EW*s and upper limits to *EW*s for all our candidate members as a function of the dereddened $(B-V)$ colors, corrected for differential reddening, as described in Prisinzano et al. (2004). Panels **b)** and **c)** show the Li *EW*s for the subsamples of the candidate members that are cluster members (panel **b)**) or contaminating field stars (panel **c)**), based on their *RV*. Our measurements are compared with the *EW*s measured for the stars in the Hyades (Sestito & Randich 2005).

4. Li analysis

4.1. Effective temperatures

As in Sestito & Randich (2005), effective temperatures were computed from the dereddened $(B-V)$ colors, using the relation $T_{\rm eff} = 1800(B-V)_0^2 - 6103(B-V)_0 + 8899$ K, given by Soderblom et al. (1993b). Since photometric errors are smaller than 0.01 mag , errors in the effective temperatures are mainly due to the interstellar reddening correction. Indeed, as discussed in Prisinzano et al. (2004), Bragaglia et al. (2006), Bonatto & Bica (2006), NGC 3960 is affected by a relatively strong

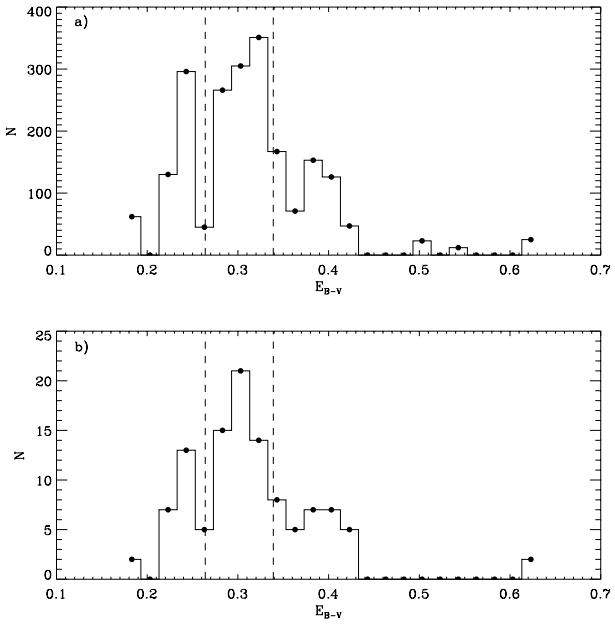

Fig. 5. Reddening distribution computed as described in Prisinzano et al. (2004), for all stars within 7 arcmin from the cluster center (panel **a**)) and for the stars observed with Giraffe (panel **b**)). The dashed lines indicate the 25th (0.26) and the 75th (0.34) percentiles of the two distributions (see text).

differential reddening. Figure 5 shows the reddening distribution computed as described in Prisinzano et al. (2004), for all stars within 7 arcmin from the cluster center (Fig. 5a) and for the stars observed with Giraffe (Fig. 5b). The dashed lines indicate the 25th (0.26) and the 75th (0.34) percentiles of the two distributions around the median value equal to 0.30; we assume the semi-difference of these two percentiles, equal to 0.04, as the typical error of $E(B-V)$. This range is in agreement with 0.29 ± 0.05 found in Bragaglia et al. (2006) and with the range [0.03, 0.34] given by Bonatto & Bica (2006).

Assuming that $\sigma_{(B-V)} \sim \sigma_{E(B-V)}$, i.e., the error in the $(B-V)$ colors corrected for differential reddening is of the order of the reddening error, we computed errors in the effective temperatures as the propagated uncertainties.

4.2. Li abundances

Li abundances were computed from the EWs and the effective temperatures by interpolating the growth curves of Soderblom et al. (1993a). Since these curves are computed assuming the local thermodynamic equilibrium (LTE), we corrected the derived Li abundance, for non-local thermodynamic equilibrium (NLTE) using the Carlsson et al. (1994) code.

Errors in Li abundances were estimated by independently computing errors in Li abundance due to the effective temperature errors and EW errors. Finally, we quadratically added these errors to estimate our uncertainties in Li abundances.

The computed Li abundances as a function of the temperatures for all the photometric candidates are shown in Fig. 6a; the RV members and the non-members are shown separately in Figs. 6b and c, respectively. Upper limits are also plotted. Final data are given in Table 4 where we list the following: identification number of Prisinzano et al. (2004), Giraffe identification name and spectrum number, celestial coordinates, V and B magnitudes, V and B magnitudes corrected for differential reddening, membership flag based on the RV (0 means "non-member", 1 means "member" and 2 means "binary"), effective temperatures computed from the $(B-V)_0$ colors, corrected for differential reddening, EW of the Li line, and finally LTE and NLTE Li abundances. Note that in some cases, the NLTE Li abundances were not computed because the LTE Li abundances were outside the range of allowed values for the Carlsson et al. (1994) correction. Note also that for the 2 binaries, the EW of the Li line were not measured due to the complexity of the spectrum of these objects.

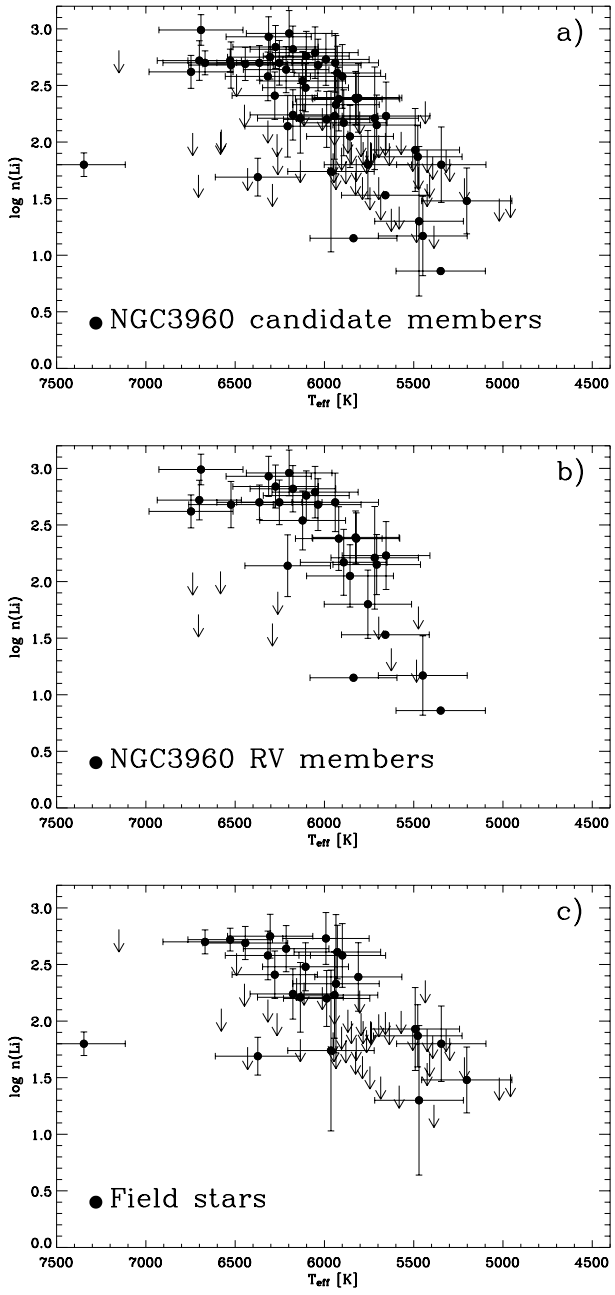

Fig. 6. Li abundances derived from the effective temperatures computed using the $(B-V)_0$ colors corrected for differential reddening, as described in Prisinzano et al. (2004). As in Fig. 4, the values are reported for the whole sample of photometric candidate members (panel **a**)) and for the subsamples of RV members and non-members (panels **b)** and **c**), respectively). Upper limits for the stars without Li are also indicated.

For comparison, Fig. 7 shows the same plots of Fig. 6, but with the Li abundances derived from the effective temperatures

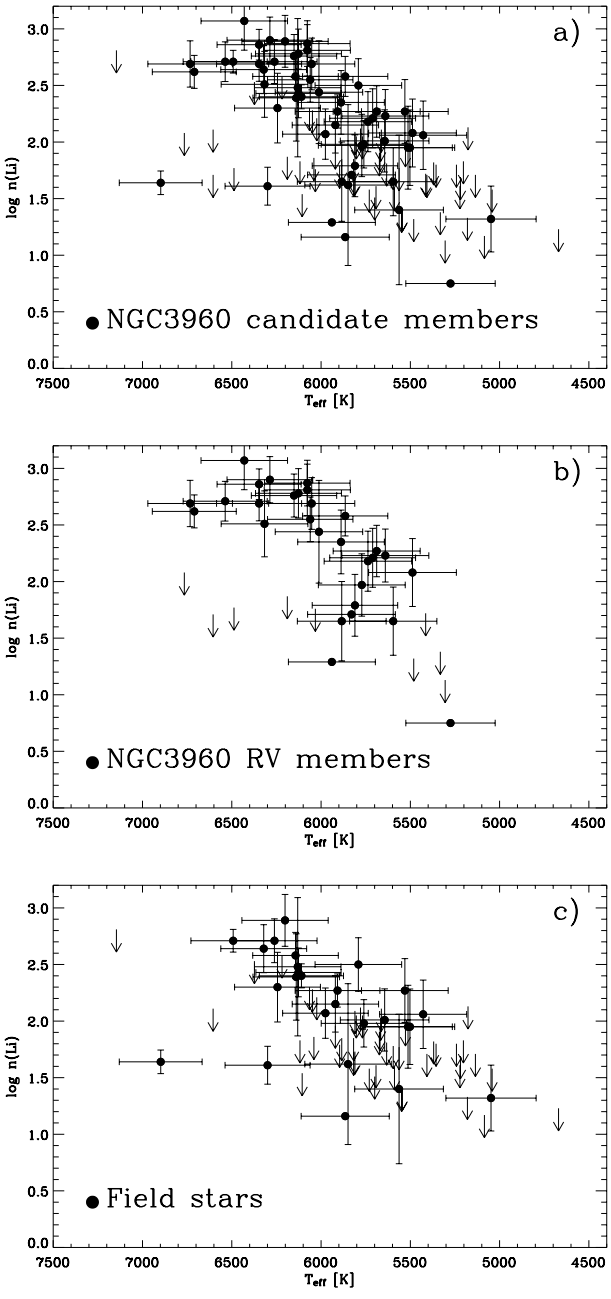

Fig. 7. Li abundances derived from the effective temperatures computed using the $(B-V)_0$ colors not corrected for differential reddening. The reported subsamples are the same described in Fig. 6.

computed using the $(B-V)_0$ colors not corrected for differential reddening.

We note that Li abundances in Fig. 7b are slightly more spread out than those in Fig. 6b. This suggests that temperatures obtained from colors corrected for differential reddening are, on average, more accurate than those from uncorrected colors; hence, we adopt them for the following analysis. However, the adopted reddening corrections are derived statistically from photometry assuming the distance of the stars of NGC 3960, therefore, the reddening correction may not be appropriate for the field stars, especially if they are foreground field stars. Nevertheless, we find that the spread in Fig. 6c is smaller than that shown in Fig. 7c and similar to that found in Pasquini et al. (1994) for field stars of similar temperatures.

5. Discussion

5.1. Li abundances

Figure 6a evidences a large spread in the Li abundance distribution: it includes both the coeval *RV* members of NGC 3960 and the inhomogeneous sample of *RV* non-members. This is especially true for F-types and later spectral types, where the amount of the Li depletion significantly depends on stellar age. In the following sections we focus on the Li distribution for cluster members and likely field stars.

5.1.1. Cluster members

Figure 6b shows the Li abundance distribution for the 29 stars with detected Li line and *RV*s consistent with membership. As already mentioned in Sect. 3.1, we estimate that a total of 39 stars are *RV* members, over a total of 113 objects studied in this work. Of the 39 objects, 16 are expected to be contaminating field stars, with *RV*s consistent with that of the cluster.

Based on Li only, we cannot definitively rule out the possibility that the 10 stars with *RV*s consistent with membership and without Li are cluster members[3]. On the one hand, for some of them we have inferred upper limit values comparable or even higher than measured Li *EW*s of stars with detected Li. On the other hand, considering these 10 objects as cluster members would imply a large spread in the Li abundances for warmer stars, which, again, we cannot completely exclude. We note however that if these 10 stars, or most of them, were indeed cluster members, most of the contaminating field stars would have high Li, which is rather unlikely. On the contrary, we make the more reasonable hypothesis that the 29 *RV* members with detected Li are cluster members, while the 10 remaining objects labeled as *RV* members, but without a detected Li line, are among the 16 contaminating stars. This assumption would imply that we have ∼60% of non-members (10/16) without a measurable Li, which is in agreement with the expected fraction of field stars without Li (see next section).

The remaining 6 contaminating field stars show the Li line but cannot be identified in the sample of the 29 members shown in Fig. 6b.

In Fig. 8 we compare the Li abundances for the 29 NGC 3960 candidate members with the Li abundances of the Hyades. The two distributions are almost identical for stars warmer than about 6000 K, while the Li abundances of NGC 3960 stars cooler than 6000 K are systematically smaller than those of Hyades members of similar temperature. This result on the one hand supports our initial assumption that NGC 3960 is older than the Hyades; on the other hand, it allows us to add a critical datapoint (see Sect. 1) on the empirical study of the evolution of Li abundance with age.

Figure 9, adapted from Sestito & Randich (2005), shows the average Li abundances as a function of age, in three different effective temperature ranges, as computed by Sestito & Randich (2005) for open clusters of different ages; the average values in the same temperature ranges derived here for NGC 3960 using the 29 *RV* members with Li are indicated in the figure and are given in Table 2. For comparison, the position of the Sun is also indicated.

For stars cooler than 5700 K (Fig. 9c), the average Li abundance in NGC 3960 is computed from only two stars and the associated error is the semi-difference of the two Li abundances.

[3] The sample of the 10 stars includes the binary with a *RV* consistent with that of the cluster, for which the *EW* has not been measured.

Table 2. Average of log n(Li) for NGC 3960 in three different ranges of effective temperatures.

$\Delta T_{\rm eff}$	$\langle \log n(\mathrm{Li}) \rangle$	error	error type
[6050–6350] K	2.72	0.25	σ
[5750–6050] K	2.19	0.48	σ
[5500–5700] K	1.88	0.35	maximum error

As discussed in Sestito & Randich (2005), the upper panel shows that after a small amount of Li depletion occurring during the pre-main sequence (PMS) phase, no Li destruction is present up to about 250 Myr, while it restarts. The average abundances for NGC 3960 confirm the trend of slow (but present) depletion at ages older than the Hyades.

Figure 9b and c indicate that for cooler stars, after the phase of PMS Li destruction, Li depletion restarts significantly after about 200 Myr. Importantly, our analysis allows us to put tighter constraints on the age at which Li depletion is no longer present. Specifically, the average Li abundances derived for NGC 3960 shows that the Li plateau might start at ∼1 Gyr rather than 2 Gyr: the average abundance of NGC 3960 is indeed closer to that of the 2 Gyr clusters, rather than to the Hyades, although, due to the large σ, it is not completely inconsistent with the latter. Also, average Li abundances in NGC 3960 could be lowered by the inclusion of a few non-members with *RV*s consistent with that of NGC 3960 but, which might have lower Li abundances. For example, the average Li abundance of stars in Fig. 9b has been computed, including in the sample the star with log n(Li) $\simeq$ 1.15 and $T_{\rm eff} \simeq$ 5800 K; its Li abundance significantly deviates from the mean Li pattern, suggesting that this object might come from the sample of contaminating field stars. By excluding this object from the sample we would get a smaller σ (0.31) and a slightly higher average (2.32), which is however consistent with that of older clusters.

We stress that our analysis has been carried out consistently with that of Sestito & Randich (2005) and thus the comparison of the average abundances should not be affected by systematic errors.

As discussed by Sestito & Randich (2005), none of the models/mechanisms proposed to explain the occurrence of MS Li depletion is also able to reproduce the plateau, since all of them predict that Li depletion should continue at old ages. To our knowledge, no new models predicting the existence of the plateau have been presented. Our study, not only reinforces the empirical evidence for the plateau and thus the need for such models, but also provides an additional constraint to be taken into account.

5.1.2. Field stars

Figure 6c shows the Li abundance distribution for the 26 objects that are contaminating field stars according to their *RV*, but do show the Li line. Their distribution is not remarkably different from that of NGC 3960 members, although it is characterized by a much larger dispersion. As discussed in Prisinzano et al. (2004), the differential reddening correction was computed as the distance (along the reddening vector) of the position in the CMD of each star from the assumed MS at the cluster distance. Therefore, such correction does not take into account the distance spread from the Sun for field stars and this explains the large spread in the Li abundance.

Nevertheless, several stars with high abundance (log n(Li) > 2) are present. More specifically, we find that the field stars hotter than about 6400 K (early F-type) show a Li abundance of about 2.7, consistent with that found for stars of similar temperatures for NGC 3960; stars cooler than 6400 K and hotter than 5700 K (late F-type and early G-type) show a large spread in the Li abundance with values similar or smaller than those found for the same temperature range for NGC 3960; finally, stars with temperatures smaller than about 5500 K have Li abundances somewhat larger than those found for NGC 3960. Note, however, that effective temperatures (and thus Li abundances) for these stars might have been overestimated, since we have assumed the same reddening as for NGC 3960 members.

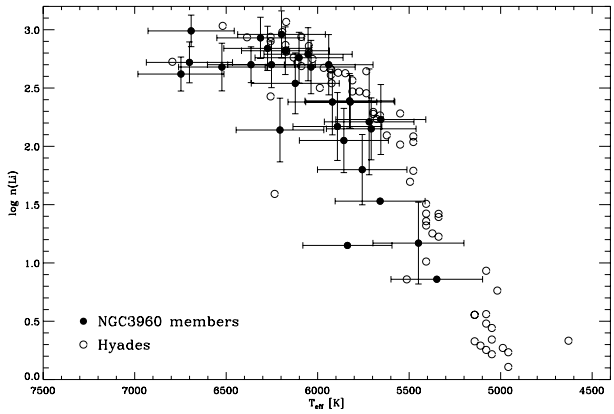

Fig. 8. Li abundances of the 29 NGC 3960 members (filled circles) as in Fig. 6 (panel **b**)), compared with the Hyades values (empty circles).

We exclude that the stars in Fig. 6c are binary cluster members (SB1) with discrepant *RV*s due to the orbital component, since for these objects, the distribution of the difference between the maximum and the minimum values of the *RV* measured from our spectra (acquired within about one and a half months, see Table 1) is very similar to that obtained for the sample of *RV* members. Therefore, we conclude that they are, most likely, a sample of field stars with Li.

If we consider that we have 74 non-members for *RV* (i.e. 113-39), including the binary, plus 16 contaminating field stars stars with *RV*s consistent with that of NGC 3960, we have a total of 90 field stars; those with the Li line are 26 within the sample of *RV* non members, plus the remaining 6 contaminating field stars in the sample of *RV* members. Therefore, the fraction of field stars with the Li line is (26+6)/90, i.e., about one third of the sample. This fraction is slightly lower than that found by Pasquini et al. (1994), who found that about one half of the G dwarfs analyzed in their work had high Li content ($2.0 \lesssim \log n(\mathrm{Li}) \lesssim 3.0$) and apparently old age. Also note that all solar-type stars in the very old cluster NGC 188 (∼6 Gyr) with available Li measurements have abundances above 2.0 (Randich et al. 2003), i.e., a relatively high Li is not inconsistent with a very old age.

In summary, the presence of several Li-rich F and G-type field stars in our sample is not surprising. The large spread in their Li abundance is both consistent with a mixed population of stars older or similar to NGC 3960, and also possibly/in part due to the fact that, in addition to stellar age, another unknown parameter can regulate MS Li depletion (e.g. Pasquini et al. 1994; Pinsonneault 1997; Pasquini et al. 1997; Charbonnel & Talon 2005; Randich et al. 2006, and references therein).

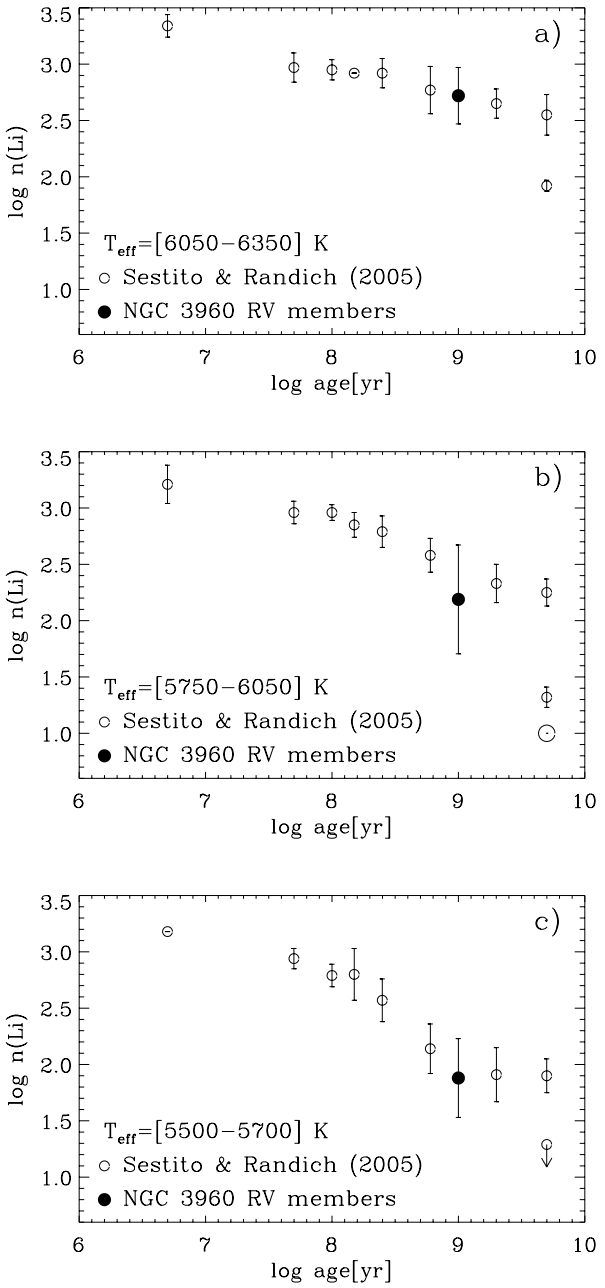

Fig. 9. Plots adapted from Fig. 7 of Sestito & Randich (2005) showing the average log n(Li) as a function of cluster age, in three different temperature ranges. Open circles are the data from Sestito & Randich (2005), while filled circles are the values computed for NGC 3960.

5.2. Membership and contamination

Table 3 gives the total number of stars defined as cluster members or non-members based on the *RV* and the presence or not of the Li line in their spectrum. As already discussed in the previous section, we find a total of 29 objects that satisfy both membership criteria. This sample contains 6 of the 16 contaminating stars with *RV*s consistent with that of NGC 3960, estimated by the *RV* distribution of the field stars (see Sect. 3.1). The remaining 10 contaminating stars can be individually distinguished since they do not show the Li line. If we add the 74 stars with *RV*s not consistent with the cluster membership, we have a total of 84 individually known non-members over a total of 113 observed stars.

Table 3. Number of stars with *RV* consistent or not (within 3σ) with the cluster membership (indicated by *Y* or *N*) and with or without Li (indicated by *Y* or *N*). The total number for each criterion is also given. The two binaries are specifically indicated in the given samples.

Li \ *RV*	*Y*	*N*	Tot.
Y	29	26	55
N	10(9 + 1)	48(47 + 1)	58(56 + 2)
Tot.	39(38 + 1)	74(73 + 1)	113(111 + 2)

We considered these 84 objects to estimate the fraction of contaminating field stars in our sample as a function of the *V* magnitude. The results are shown by the solid line histogram plotted in Fig. 10; the number of contaminating stars and the total number of objects within the four magnitude ranges are also indicated; error bars were computed from the binomial distribution. The resulting fractions are compared with the analogous values derived in Prisinzano et al. (2004), where the contamination was statistically derived using a field region outside the cluster region; in this case, errors were computed from the propagation of the poisson errors on the number of field stars and of the total stars. The comparison shows that, within the errors, the fractions of contaminating stars derived with the two methods are compatible.

We note, however, that, among the 84 contaminating stars, the sample of 74 non-members for the *RV* could include a *small* fraction of binaries of NGC 3960, therefore these numbers could be slightly overestimated. On the other hand, we did not include in the field star sample the 6 contaminating stars with *RV*s consistent with that of the cluster and with the Li line. Nevertheless, since these effects should be within the error bars, we conclude that the fraction of contaminating field stars within the spectroscopic sample studied in this work is comparable with that estimated in Prisinzano et al. (2004) with photometric data. We note that the comparison is consistent since the stars observed in this spectroscopic work have been randomly selected from the list of photometric candidate members given in Prisinzano et al. (2004). This result allows us to confirm the mass function derived in Prisinzano et al. (2004), which strongly depends on the correction for the field star contamination.

6. Summary and conclusions

We used VLT/FLAMES Giraffe spectra to determine the *RV*s and thus the membership of a sample of 113 photometrically selected candidate cluster members. We find that the average cluster *RV* is $-20.0 \pm 0.7\,\mathrm{km\,s^{-1}}$ with a standard deviation $\sigma = 2.3 \pm 0.6\,\mathrm{km\,s^{-1}}$. As expected from the high fraction of contaminating stars, only 39 objects have *RV*s consistent with that of the cluster. Among these, 16 are expected to be contaminating field stars and 10 of these have been identified since they do not show the Li line. We find that the spread in the CMD for the sample of cluster members is not reduced since the adopted reddening correction is statistically reliable. Individual spectral types of such objects are necessary to accurately derive their temperatures and positions in the CMD.

From the analysis of the Li line we derived Li abundances for cluster and field stars. We find that by using photometry corrected for differential reddening, Li abundance distribution of the cluster members shows a spread smaller than that found using uncorrected photometry.

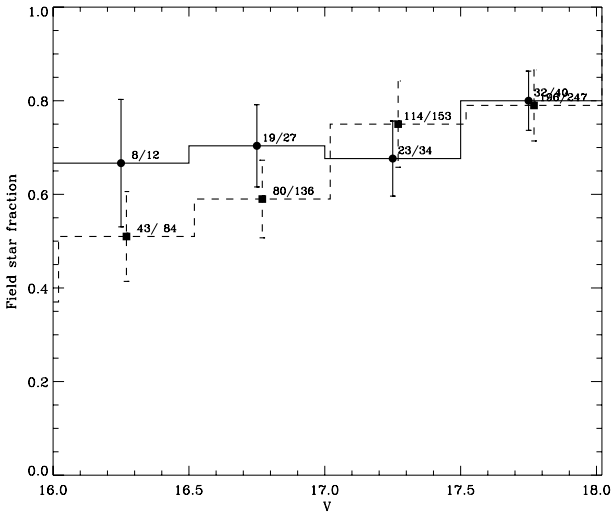

Fig. 10. Fraction of contaminating field stars estimated in this work from individual membership derived by the *RV* and the Li line (solid line histogram) and in Prisinzano et al. (2004) from a statistical analysis of a field region around NGC 3960 (dashed line histogram).

The average Li abundances computed for stars in three different temperature ranges confirms the trend, already found in Sestito & Randich (2005), of slow (but present) depletion at ages older than the Hyades for stars with temperatures larger than about 6000 K. For cooler stars, the inclusion of the average Li abundance of NGC 3960 in the distribution of Li abundance as a function of the age, allows us to conclude that the age at which Li depletion is no longer present is very likely closer to 1 Gyr rather than 2 Gyr, as inferred by Sestito & Randich (2005), on the base of the incomplete sample of open clusters with ages older than 2 Gyr and younger than the Hyades.

The fraction of field stars with an evident Li line is about one third, while the fraction of field stars, as a function of the magnitude, is consistent with that derived statistically from photometry. This allows us to confirm the conclusions about the mass function derived in Prisinzano et al. (2004), which strongly depends on the estimate of the field star contamination.

Acknowledgements. We wish to thank the referee R. D. Jeffries for his useful suggestions which have improved the final version of this paper. We also thank the ESO Paranal staff for performing the service mode observations. This work has made extensive use of the services of WEBDA, ADS, CDS etc. The research presented here has been supported by an INAF grant on *Stellar clusters as probes of star formation and early stellar evolution (PI: F. Palla)*. L.P. thanks Paolo Spanò for his contribution to the *RV* analysis and Giusi Micela for useful discussions on this work.

References

Blecha, A., & Simond, G. 2004, Technical report (GIRAFFE BLDR Software – Reference Manual Version 1.12, Observatoire de Geneve)
Bonatto, C., & Bica, E. 2006, A&A, 455, 931
Bragaglia, A., Tosi, M., Carretta, E., et al. 2006, MNRAS, 366, 1493
Carlsson, M., Rutten, R. J., Bruls, J. H. M. J., & Shchukina, N. G. 1994, A&A, 288, 860
Charbonnel, C., & Talon, S. 2005, Science, 309, 2189
Friel, E. D., & Janes, K. A. 1993, A&A, 267, 75
Jeffries, R. D., & Oliveira, J. M. 2005, MNRAS, 358, 13
Pallavicini, R., Spanò, P., Prisinzano, L., et al. 2006, Multi-Object Spectroscopy of Open Clusters with FLAMES: Preliminary GTO Results, Chemical Abundances and Mixing in Stars in the Milky Way and its Satellites, ESO Astrophysics Symposia (Springer-Verlag), 181
Pasquini, L., Liu, Q., & Pallavicini, R. 1994, A&A, 287, 191
Pasquini, L., Randich, S., & Pallavicini, R. 1997, A&A, 325, 535
Pinsonneault, M. 1997, ARA&A, 35, 557
Prisinzano, L., Micela, G., Sciortino, S., & Favata, F. 2004, A&A, 417, 945
Prisinzano, L., Damiani, F., Micela, G., & Pillitteri, I. 2007, A&A, 462, 123
Randich, S., Sestito, P., & Pallavicini, R. 2003, A&A, 399, 133
Randich, S., Bragaglia, A., Pastori, L., et al. 2005, The Messenger, 121, 18
Randich, S., Sestito, P., Primas, F., et al. 2006, A&A, 450, 557
Sestito, P., & Randich, S. 2005, A&A, 442, 615
Sestito, P., Bragaglia, A., Randich, S., et al. 2006, A&A, 458, 121
Soderblom, D. R., Oey, M. S., Johnson, D. R. H., & Stone, R. P. S. 1990, AJ, 99, 595
Soderblom, D. R., Jones, B. F., Balachandran, S., et al. 1993a, AJ, 106, 1059
Soderblom, D. R., Stauffer, J. R., Hudon, J. D., & Jones, B. F. 1993b, ApJS, 85, 315
Soderblom, D. R., Jones, B. F., Stauffer, J. R., & Chaboyer, B. 1995, AJ, 110, 729
Sozzetti, A., Torres, G., Charbonneau, D., et al. 2007, ApJ, 664, 1190
Thorburn, J. A., Hobbs, L. M., Deliyannis, C. P., & Pinsonneault, M. H. 1993, ApJ, 415, 150
Tonry, J., & Davis, M. 1979, AJ, 84, 1511

Online Material

Table 4. Stellar parameters for the NGC 3960 stars observed with GIRAFFE. Col. 1 gives the identification number of Prisinzano et al. (2004), Cols. 2 and 3 give the Giraffe identification name and the spectrum number, Cols. 4 and 5 give the celestial coordinates, Cols. 6 and 7 give the V and B magnitudes while Cols. 8 and 9 give the V and B magnitudes corrected for differential reddening, Col. 11 gives the membership flag based on the RV (0 means "non member", 1 means "member" and 2 means "binary"); Col. 12 gives the effective temperatures computed from the $(B-V)_0$ colors, corrected for differential reddening; Col. 13 gives the EW of the Li line and finally Col. 14 and 15 give the LTE and NLTE Li abundances, respectively.

ID P04	ID Giraffe	Sp	RA(2000) [deg]	Dec(2000) [deg]	V	B	Vcor	Bcor	RV [km/s]	M. RV	Teff [K]	EW(Li) mÅ	log n(Li) LTE	log n(Li) NLTE
301398	OC21-M104	2	177.61640930	-55.64477921	16.594± 0.003	17.514± 0.006	16.527	17.425	-16.85± 1.60	1	5771± 243	34± 4	2.04	2.05± 0.28
301121	OC21-M80	3	177.64503479	-55.66763687	16.388± 0.004	16.995± 0.003	16.387	16.993	-1.95± 5.21	0	7146± 232	< 50	< 2.89	< 2.81
301726	OC21-M301	4	177.62678528	-55.60786819	17.435± 0.003	18.420± 0.005	17.130	18.017	-36.28± 0.91	0	5530± 242	84±11	2.61	2.58± 0.28
301718	OC21-M299	5	177.61761475	-55.61308289	16.645± 0.003	17.555± 0.006	16.340	17.152	-15.42± 0.67	1	5810± 239	25± 3	2.17	2.14± 0.27
301899	OC21-M339	6	177.63058472	-55.60299683	16.935± 0.003	17.771± 0.003	16.701	17.461	-4.28± 0.99	0	6105± 237	< 5	< 1.81	< 1.77
301886	OC21-M566	7	177.53912354	-55.58911514	17.900± 0.005	19.030± 0.006	17.749	18.830	2.16± 0.70	0	5048± 252	38± 0	1.36	1.48± 0.29
301897	OC21-M571	8	177.57386780	-55.57822037	17.830± 0.004	18.785± 0.005	17.679	18.585	-20.03± 1.10	1	5640± 243	68± 3	2.40	2.39± 0.23
301352	OC21-M260	9	177.58436584	-55.64488983	17.454± 0.003	18.284± 0.007	17.600	18.478	-42.39± 3.37	0	6130± 242	51±17	2.34	2.33± 0.61
301058	OC21-M65	10	177.63095093	-55.67090225	16.949± 0.002	17.792± 0.003	16.858	17.672	-19.58± 1.53	1	6076± 239	109± 0	3.06	2.96± 0.20
301407	OC21-M273	11	177.59687805	-55.63789749	16.345± 0.002	17.066± 0.004	16.278	16.977	-15.49± 7.73	1	6604± 235	< 4	< 1.76	< 1.71
301052	OC21-M64	12	177.60379028	-55.67435837	16.620± 0.002	17.445± 0.005	16.529	17.325	-20.82± 0.44	1	6151± 238	81± 0	2.92	2.84± 0.19
301654	OC21-M540	13	177.51084900	-55.60569763	17.953± 0.004	18.901± 0.007	17.928	18.868	15.99± 3.48	0	5666± 245	< 34	< 2.03	< 2.06
301928	OC21-M340	14	177.66407776	-55.59788513	17.095± 0.003	18.064± 0.004	16.857	17.749	13.11± 10.88	0	5588± 242	< 15	< 1.82	< 1.83
301430	OC21-M108	15	177.64192200	-55.65436554	16.659± 0.003	17.458± 0.004	16.628	17.417	-40.03± 1.94	0	6260± 238	65± 4	2.81	2.75± 0.19
301158	OC21-M88	16	177.71395874	-55.67267227	17.806± 0.007	18.711± 0.006	17.946	18.896	-20.29± 0.98	1	5829± 245	22± 9	1.49	1.53± NaN
301901	OC21-M572	17	177.63180542	-55.59672165	17.675± 0.004	18.651± 0.004	17.441	18.341	9.99± 1.55	0	5563± 243	< 23	< 1.99	< 2.00
301874	OC21-M564	18	177.58049011	-55.60188675	16.933± 0.004	17.801± 0.005	16.782	17.601	-8.75± 0.52	0	5975± 239	30± 2	2.27	2.24± 0.22
301933	OC21-M581	19	177.64627075	-55.59481430	17.922± 0.004	19.011± 0.007	17.684	18.696	-1.25± 6.67	0	5176± 248	< 100	< 2.33	< 2.36
302027	OC21-M607	20	177.59971619	-55.57306290	16.706± 0.002	17.624± 0.003	16.521	17.380	4.67± 0.69	0	5779± 241	< 35	< 2.32	< 2.30
301504	OC21-M125	21	177.69602966	-55.65551758	17.305± 0.004	18.381± 0.006	17.501	18.640	-0.97± 0.71	0	5219± 256	< 39	< 1.35	< 1.50
301395	OC21-M102	22	177.61032104	-55.64798737	17.641± 0.003	18.700± 0.009	17.574	18.611	-20.30± 0.77	1	5274± 250	16± 3	0.77	0.86± NaN
301801	OC21-M327	23	177.74018860	-55.60593796	18.074± 0.004	19.338± 0.008	17.752	18.912	55.82± 1.38	0	4669± 257	< 47	< 1.36	< 1.53
301796	OC21-M324	24	177.71359253	-55.60955429	16.720± 0.002	17.570± 0.003	16.398	17.144	31.76± 8.73	0	6048± 237	< 31	< 2.66	< 2.60
301961	OC21-M344	25	177.71797180	-55.60043716	18.321± 0.006	19.396± 0.027	17.953	18.909	-11.88± 6.99	0	5222± 246	< 33	< 1.95	< 1.99
301803	OC21-M328	26	177.70584106	-55.60463715	17.020± 0.002	17.956± 0.003	16.698	17.530	-20.18± 0.79	1	5710± 240	58± 8	2.58	2.54± 0.26
301792	OC21-M323	28	177.73258972	-55.61131668	17.810± 0.006	18.824± 0.006	17.488	18.398	-4.05± 0.74	0	5428± 243	69±10	2.40	2.39± 0.30
301132	OC21-M83	29	177.66281128	-55.65973282	17.232± 0.003	18.140± 0.004	17.231	18.138	36.26± 1.15	0	5817± 243	< 17	< 1.83	< 1.85
301935	OC21-M342	30	177.67820740	-55.59440231	16.430± 0.003	17.209± 0.018	16.192	16.894	-24.19± 1.07	1	6346± 235	77± 8	3.08	2.99± 0.14
302057	OC21-M618	31	177.69938660	-55.56567001	17.618± 0.005	18.514± 0.007	17.281	18.068	-20.67± 1.75	1	5864± 238	89± 2	3.02	2.93± 0.18
301563	OC21-M282	33	177.79658508	-55.64903641	17.703± 0.006	18.652± 0.004	17.936	18.960	-5.83± 2.56	0	5662± 249	< 41	< 1.80	< 1.87
301596	OC21-M286	34	177.79386902	-55.64278793	17.598± 0.030	18.420± 0.006	17.831	18.728	-2.50± 3.12	2	6163± 243			
301590	OC21-M284	36	177.79833984	-55.63433838	16.956± 0.002	17.852± 0.003	17.189	18.160	7.00± 0.99	0	5864± 246	12± 1	0.62	NaN± NaN
301534	OC21-M279	37	177.77566528	-55.63899612	17.032± 0.002	17.888± 0.003	17.258	18.186	15.58± 0.56	0	6023± 244	< 28	< 1.98	< 2.00
301810	OC21-M331	38	177.77940369	-55.62976456	16.948± 0.004	17.738± 0.006	16.893	17.666	-43.74± 1.48	0	6299± 238	11± 0	1.72	1.69± 0.17
301097	OC21-M76	39	177.64811707	-55.68087006	17.423± 0.004	18.422± 0.012	17.422	18.420	-19.59± 0.64	1	5480± 248	< 10	< 1.25	< 1.31
301821	OC21-M336	41	177.76026917	-55.62009811	18.044± 0.005	18.935± 0.007	17.989	18.863	-39.11± 1.93	0	5884± 242	< 16	< 1.90	< 1.90
301827	OC21-M337	42	177.75772095	-55.61386490	16.698± 0.003	17.610± 0.002	16.643	17.538	-8.92± 0.46	0	5802± 243	< 28	< 2.10	< 2.10
301540	OC21-M281	43	177.76679993	-55.63492203	17.670± 0.004	18.617± 0.005	17.896	18.915	167.15± 1.77	0	5669± 249	< 28	< 1.64	< 1.71
301830	OC21-M338	44	177.74417114	-55.60812378	18.028± 0.014	19.097± 0.011	17.973	19.025	12.22± 2.51	0	5241± 251	< 47	< 1.76	< 1.85
300910	OC21-M217	45	177.79577637	-55.69689941	17.625± 0.004	18.434± 0.003	17.945	18.857	17.85± 2.41	0	6218± 243	< 47	< 2.27	< 2.27

Table 4. continued.

ID P04	ID Giraffe	Sp	RA(2000) [deg]	Dec(2000) [deg]	V	B	Vcor	Bcor	RV [km/s]	M. RV	Teff [K]	EW(Li) mÅ	log n(Li) LTE	log n(Li) NLTE
300747	OC21-M35	46	177.68829346	-55.69499588	17.286± 0.030	18.129± 0.010	17.306	18.155	-18.22± 2.96	1	6076± 241	98± 6	2.85	2.79± 0.23
301242	OC21-M247	47	177.81761169	-55.68233490	17.522± 0.005	18.404± 0.006	17.470	18.335	22.04± 0.66	0	5919± 241	37± 4	2.21	2.20± 0.25
301258	OC21-M249	48	177.82002258	-55.66353226	16.936± 0.004	17.954± 0.003	16.884	17.885	-16.30± 0.80	1	5414± 248	< 28	< 1.72	< 1.78
301204	OC21-M238	49	177.78804016	-55.67609024	15.902± 0.002	16.687± 0.002	16.058	16.894	-6.97± 0.97	0	6321± 240	53± 2	2.51	2.48± 0.21
301227	OC21-M241	51	177.78099060	-55.66153717	16.630± 0.002	17.403± 0.002	16.786	17.610	-1.05± 0.61	0	6373± 240	< 32	< 2.41	< 2.38
301257	OC21-M248	52	177.79270935	-55.66469574	17.322± 0.006	18.138± 0.003	17.270	18.069	-23.36± 1.15	1	6189± 239	< 9	< 1.94	< 1.91
301594	OC21-M285	53	177.80053711	-55.65325165	17.676± 0.006	18.535± 0.005	17.909	18.843	-20.39± 1.36	1	6011± 244	57±15	2.19	2.21± 0.45
300530	OC21-M184	54	177.77345276	-55.72911453	16.947± 0.003	17.750± 0.003	17.026	17.855	0.26± 0.88	0	6243± 240	30± 5	2.23	2.21± 0.31
300518	OC21-M181	55	177.78697205	-55.72935104	17.707± 0.003	18.683± 0.009	17.786	18.788	-5.78± 0.92	0	5563± 248	21± 4	1.23	1.30± 0.66
300523	OC21-M182	56	177.77871704	-55.72303772	16.432± 0.002	17.309± 0.013	16.511	17.414	-15.61± 0.66	1	5939± 243	12± 2	1.13	1.15± NaN
300548	OC21-M185	57	177.79891968	-55.72080994	17.340± 0.004	18.186± 0.004	17.303	18.137	55.35± 14.08	0	6064± 240	< 32	< 2.37	< 2.34
300824	OC21-M202	58	177.78025818	-55.71140289	17.424± 0.007	18.315± 0.004	17.786	18.794	-26.33± 1.01	1	5884± 248	19± 1	1.10	1.17± 0.35
300840	OC21-M205	59	177.78459167	-55.70513535	17.080± 0.002	17.840± 0.003	17.442	18.319	-22.22± 1.26	1	6429± 242	98± 9	2.75	2.70± 0.26
300890	OC21-M213	60	177.79322815	-55.70159912	17.025± 0.003	17.811± 0.003	17.345	18.234	-21.72± 4.03	1	6316± 242	41± 6	2.17	2.17± 0.29
301241	OC21-M246	61	177.79833984	-55.68308640	16.093± 0.004	16.920± 0.004	16.041	16.851	6.53± 0.82	0	6143± 239	60± 2	2.69	2.64± 0.20
301235	OC21-M245	62	177.78887939	-55.68545532	16.942± 0.004	17.755± 0.004	17.098	17.962	-55.02± 1.12	0	6201± 241	95± 5	2.78	2.73± 0.23
300788	OC21-M48	64	177.70639038	-55.70300293	17.812± 0.011	18.793± 0.006	17.952	18.978	24.90± 2.28	0	5545± 249	< 11	< 1.18	< 1.26
300206	OC21-M137	65	177.68759155	-55.74437714	17.239± 0.004	18.121± 0.019	17.251	18.137	-0.72± 0.80	0	5919± 242	< 19	< 1.95	< 1.95
300721	OC21-M26	67	177.67782593	-55.71119690	16.037± 0.015	16.723± 0.011	16.057	16.749	-13.66± 20.71	1	6765± 235	< 10	< 2.13	< 2.08
300283	OC21-M144	68	177.75404358	-55.74374390	17.154± 0.007	17.933± 0.015	17.142	17.917	-18.09± 1.33	1	6346± 238	55± 1	2.76	2.70± 0.15
300280	OC21-M143	69	177.74539185	-55.74773788	17.948± 0.004	18.879± 0.017	17.936	18.863	-27.03± 0.78	0	5729± 244	< 11	< 1.57	< 1.60
300511	OC21-M177	70	177.76091003	-55.74037170	17.350± 0.006	18.202± 0.010	17.429	18.307	-7.65± 10.59	0	6040± 242	< 12	< 1.78	< 1.78
300762	OC21-M41	71	177.67546082	-55.69906616	16.294± 0.002	17.015± 0.002	16.314	17.041	-11.62± 3.35	0	6604± 236	< 10	< 2.16	< 2.11
300514	OC21-M178	72	177.77122498	-55.73638916	17.212± 0.008	18.005± 0.007	17.291	18.110	-22.26± 1.08	1	6286± 239	89± 2	2.89	2.82± 0.20
300274	OC21-M401	73	177.75950623	-55.75041580	16.973± 0.002	17.806± 0.008	16.961	17.790	-7.78± 0.79	0	6118± 240	< 10	< 1.86	< 1.84
300486	OC21-M169	75	177.69763184	-55.73072052	17.872± 0.005	18.852± 0.010	17.842	18.813	3.18± 0.99	0	5548± 246	< 10	< 1.38	< 1.43
300198	OC21-M134	76	177.65122986	-55.75020218	17.454± 0.004	18.393± 0.004	17.466	18.409	22.26± 0.98	0	5699± 245	< 10	< 1.47	< 1.51
300203	OC21-M136	77	177.64178467	-55.74533844	16.530± 0.002	17.242± 0.003	16.542	17.258	-20.79± 2.03	2	6645± 236			
300048	OC21-M353	78	177.67778015	-55.77682877	17.291± 0.027	18.179± 0.006	17.012	17.810	-2.31± 2.87	0	5895± 239	< 13	< 2.10	< 2.07
300073	OC21-M359	79	177.69346619	-55.78541565	18.068± 0.006	19.065± 0.012	17.924	18.875	-20.60± 0.98	1	5487± 245	65± 9	2.21	2.23± 0.30
300085	OC21-M362	81	177.71144104	-55.77383804	17.295± 0.003	18.142± 0.003	17.151	17.952	-23.75± 1.04	1	6060± 239	65± 1	2.76	2.70± 0.20
300814	OC21-M58	82	177.69410706	-55.70250320	16.188± 0.005	16.935± 0.005	16.328	17.120	-17.04± 2.88	1	6487± 238	< 5	< 1.66	< 1.63
300794	OC21-M52	83	177.71516418	-55.70048523	17.259± 0.009	18.252± 0.004	17.399	18.437	-35.63± 4.61	0	5502± 250	51± 7	1.72	1.80± 0.33
300727	OC21-M29	84	177.67022705	-55.70906830	17.090± 0.007	17.921± 0.005	17.110	17.947	-20.57± 1.19	1	6126± 240	88± 4	2.82	2.76± 0.22
300670	OC21-M200	86	177.60665894	-55.71213531	17.730± 0.005	18.640± 0.010	17.621	18.496	16.29± 2.03	0	5810± 242	< 14	< 1.84	< 1.84
300128	OC21-M375	87	177.57582092	-55.76447678	17.765± 0.004	18.815± 0.007	17.482	18.441	-16.76± 0.70	1	5305± 246	< 9	< 1.36	< 1.41
300201	OC21-M135	88	177.67399597	-55.74694443	16.737± 0.005	17.586± 0.002	16.749	17.602	-21.75± 0.76	1	6052± 241	83± 5	2.73	2.68± 0.23
300666	OC21-M14	89	177.62507629	-55.71351624	17.924± 0.005	19.005± 0.006	17.815	18.861	11.37± 0.68	0	5202± 250	< 54	< 1.85	< 1.93
300680	OC21-M16	91	177.63342285	-55.70466995	17.508± 0.004	18.450± 0.004	17.399	18.306	-20.72± 3.14	1	5688± 243	66± 1	2.38	2.38± 0.23
300745	OC21-M34	93	177.66360474	-55.69713211	17.902± 0.005	18.892± 0.006	17.922	18.918	12.63± 1.32	0	5512± 248	49± 9	1.87	1.93± 0.37
300364	OC21-M150	95	177.58456421	-55.72017670	17.111± 0.003	18.131± 0.003	16.831	17.760	-27.53± 0.92	0	5407± 244	< 28	< 1.97	< 1.99
300326	OC21-M416	96	177.50790405	-55.72454453	17.978± 0.004	19.066± 0.006	16.946	17.702	144.01± 1.26	0	5180± 237	< 18	< 2.38	< 2.33
300427	OC21-M160	97	177.64410400	-55.73705292	17.461± 0.007	18.390± 0.006	17.483	18.420	-23.74± 1.87	1	5737± 245	52± 5	2.13	2.15± 0.27

Table 4. continued.

ID P04	ID Giraffe	Sp	RA(2000) [deg]	Dec(2000) [deg]	V	B	Vcor	Bcor	RV [km/s]	M. RV	Teff [K]	EW(Li) mÅ	log n(Li) LTE	log n(Li) NLTE
300123	OC21-M374	100	177.54367065	-55.76549911	17.152± 0.018	17.810± 0.119	16.869	17.436	-4.26± 1.24	0	6897± 231	8± 0	1.87	1.80± 0.10
300211	OC21-M138	101	177.68962097	-55.75462341	17.671± 0.005	18.581± 0.007	17.683	18.597	9.69± 1.74	0	5810± 244	< 30	< 2.06	< 2.07
300700	OC21-M19	103	177.59857178	-55.69359970	18.020± 0.007	18.961± 0.006	17.911	18.817	-5.53± 1.21	0	5692± 243	< 13	< 1.71	< 1.73
300435	OC21-M162	106	177.64506531	-55.73121643	16.789± 0.002	17.697± 0.003	16.811	17.727	17.82± 0.34	0	5817± 244	< 13	< 1.67	< 1.69
300652	OC21-M196	107	177.54794312	-55.69823456	17.456± 0.004	18.341± 0.008	17.059	17.816	-69.91± 1.16	0	5907± 237	49± 3	2.75	2.69± 0.15
300647	OC21-M195	108	177.55949402	-55.69301224	17.194± 0.018	18.117± 0.005	16.797	17.592	0.51± 1.21	0	5760± 238	35± 2	2.45	2.41± 0.21
300636	OC21-M192	109	177.55455017	-55.70640182	17.085± 0.003	17.939± 0.009	16.688	17.414	-20.18± 1.21	1	6032± 236	< 10	< 2.14	< 2.09
300330	OC21-M419	110	177.48760986	-55.71766663	18.232± 0.005	19.350± 0.010	17.200	17.986	4.69± 1.11	0	5085± 238	< 16	< 2.22	< 2.19
300633	OC21-M190	111	177.57122803	-55.70737076	18.154± 0.010	19.256± 0.007	17.757	18.731	30.50± 0.53	0	5135± 246	< 48	< 2.05	< 2.09
300576	OC21-M443	112	177.47384644	-55.70010757	18.047± 0.005	19.179± 0.005	17.682	18.697	3.41± 0.88	0	5042± 249	< 44	< 1.86	< 1.93
300694	OC21-M18	113	177.63012695	-55.69725800	17.749± 0.007	18.706± 0.007	17.640	18.562	54.13± 4.03	0	5632± 244	< 23	< 1.90	< 1.92
300627	OC21-M187	114	177.56176758	-55.71266174	17.025± 0.002	17.860± 0.003	16.628	17.335	-10.28± 1.21	0	6109± 235	45± 4	2.77	2.70± 0.11
300943	OC21-M471	116	177.47677612	-55.66456985	17.266± 0.003	18.233± 0.004	17.135	18.059	-13.38± 1.38	1	5595± 244	27± 3	1.78	1.80± 0.30
301000	OC21-M224	117	177.57020569	-55.67611313	17.402± 0.003	18.356± 0.004	17.543	18.543	-5.23± 0.67	0	5643± 248	45± 3	1.81	1.87± 0.27
301327	OC21-M508	118	177.48970032	-55.65196609	16.499± 0.008	17.235± 0.004	16.387	17.087	-17.68± 1.61	1	6536± 235	46± 7	2.79	2.72± 0.18
300935	OC21-M467	119	177.47935486	-55.68232727	18.121± 0.008	19.156± 0.013	17.990	18.982	20.55± 2.15	0	5355± 247	< 38	< 1.89	< 1.94
301020	OC21-M230	120	177.56149292	-55.66584015	16.318± 0.002	17.011± 0.003	16.459	17.198	-19.10± 1.80	1	6733± 236	44± 7	2.75	2.68± 0.20
300712	OC21-M22	121	177.59326172	-55.68819809	18.074± 0.007	18.989± 0.010	17.965	18.845	-10.22± 1.34	0	5790± 242	84± 5	2.64	2.61± 0.24
301335	OC21-M253	122	177.55290222	-55.65553665	17.481± 0.006	18.448± 0.005	17.627	18.642	1.75± 0.53	0	5595± 249	< 22	< 1.56	< 1.63
301085	OC21-M74	123	177.59184265	-55.68221664	17.257± 0.006	18.203± 0.007	17.166	18.083	17.36± 0.85	0	5673± 244	< 26	< 1.98	< 2.00
300988	OC21-M219	124	177.56431580	-55.68196869	17.644± 0.005	18.675± 0.007	17.785	18.862	2.83± 4.57	0	5369± 252	< 38	< 1.57	< 1.68
301695	OC21-M548	126	177.57238770	-55.60731888	16.782± 0.002	17.703± 0.004	16.642	17.518	40.61± 0.55	0	5767± 242	< 29	< 2.18	< 2.17
301360	OC21-M264	127	177.57380676	-55.64166260	16.894± 0.005	17.722± 0.006	17.040	17.916	36.76± 0.60	0	6138± 242	42± 9	2.24	2.23± 0.38
301643	OC21-M535	128	177.53494263	-55.61775208	17.848± 0.004	18.738± 0.005	17.823	18.705	-23.78± 5.09	1	5888± 242	58± 8	2.39	2.38± 0.28
301076	OC21-M70	129	177.61021423	-55.66328049	17.292± 0.003	18.192± 0.003	17.201	18.072	-6.54± 0.88	0	5848± 242	19± 5	1.74	1.74± 0.71
301657	OC21-M541	130	177.50421143	-55.61781311	16.557± 0.026	17.255± 0.003	16.532	17.222	-15.43± 2.70	1	6709± 235	38± 5	2.69	2.62± 0.15
301627	OC21-M530	131	177.52270508	-55.62816620	16.615± 0.003	17.361± 0.003	16.590	17.328	16.29± 3.27	0	6491± 236	47± 2	2.79	2.72± 0.10
301316	OC21-M504	133	177.50120544	-55.63993454	17.890± 0.007	18.876± 0.007	17.778	18.728	-8.20± 0.76	0	5527± 245	< 40	< 2.05	< 2.08
301691	OC21-M547	134	177.53811646	-55.61053085	17.980± 0.005	18.811± 0.005	17.840	18.626	13.99± 2.50	0	6126± 238	47± 5	2.63	2.58± 0.22
301283	OC21-M491	135	177.48237610	-55.65919113	18.026± 0.021	19.068± 0.007	17.707	18.647	-17.28± 0.89	1	5331± 245	< 16	< 1.66	< 1.69